Int. J. Multiphase Flow Vol. 18, No. 3, pp. 313–326, 1992
Printed in Great Britain.

0301-9322/92 $5.00 + 0.00

EXPERIMENTAL INVESTIGATION OF UPWARD GAS–LIQUID FLOW IN A VERTICAL NARROW ANNULUS

V. E. NAKORYAKOV, V. V. KUZNETSOV and O. V. VITOVSKY
Institute of Thermophysics of the Siberian Branch of the Russian Academy of Sciences,
1 Academician Lavrentyev Ave, 630090 Novosibirsk, Russia

(Received 11 December 1990; in revised form 28 October 1991)

Abstract—Flow structures in vertical upward two-phase flow in a concentric narrow annular channel have been studied. A map of flow patterns has been drawn. The frictional loss has been measured for the two-phase flow over a wide range of superficial liquid and gas velocities. A mathematical model predicting frictional loss has been developed.

Key Words: gas–liquid flow, annulus, narrow gap, flow patterns, frictional loss

INTRODUCTION

Two-phase flow in an annular channel is frequently encountered in important applications such as heat exchangers with double pipes, water-cooled power supplies and oil and gas production. Despite the fact that the hydrodynamics of upward gas–liquid flow in vertical pipes has been considered in many works (Wallis 1969; Hewitt & Hall-Taylor 1970; Hewitt 1982 etc.), the number of studies on such flow in annular channels is very small (Sadatomi *et al.* 1982; Kelessidis & Dukler 1989; Caetano *et al.* 1989a, b).

The flow pattern map for upward two-phase flow in an annular channel of 15 mm i.d. and 30 mm o.d. was obtained by Sadatomi *et al.* (1982). They also obtained experimental data on the bubble rise velocity and pressure drops, well-accounted for by the well-known Lockhart & Martinelli (1949) relationship. A detailed analysis of the flow pattern map for upward two-phase flow in an annular channel of 50.8 mm i.d. and 76.2 mm o.d. was performed by Kelessidis & Dukler (1989). In all these works and in recent works by Caetano *et al.* (1989a, b), the width of the channel through which the two-phase flow passed was much larger than the capillary constant, equal to $[2\sigma/(\rho_L - \rho_G)g]^{0.5}$, so that the flow parameters were close to those in a circular pipe. Here σ, ρ_L, ρ_G and g are the surface tension, the liquid and gas densities and the gravitational acceleration, respectively. For channels with a smaller gap this constant is incorrect and the capillary forces will define the structure of the two-phase flow. There is no guarantee that the correlation for circular pipes will continue to apply in such channels. Therefore, attention should be directed toward the pressure drop and pattern problems. A better understanding of the two-phase flow in a narrow annulus with a gap much smaller than its diameter provides more reliable design methods for many types of industrial equipment with other types of narrow channels e.g. compact heat exchangers, steam generators and condensers. In the present work, upward two-phase flow has been studied in a narrow annular channel whose gap thickness was smaller than the capillary constant. Experimental data on the flow structure at different velocities as well as on the friction factor of the two-phase flow have been obtained. A method for calculation of the friction factor has been suggested.

EXPERIMENT

The experimental apparatus was a closed hydrodynamical contour, shown in figure 1. It consisted of a thermostat tank-separator (1), a centrifugal pump (2), a working section (3) and a system for regulation and measurement of the flow rates of the working fluids—water and air.

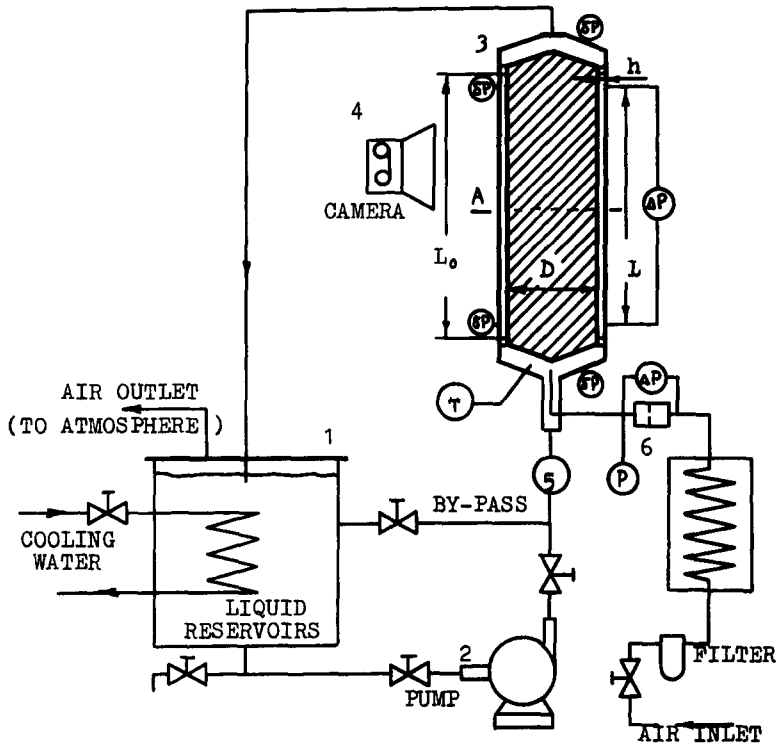

Figure 1. Experimental equipment.

The measurement section comprised two coaxial cylinders made of plexiglass with polished internal and external surfaces. This allowed visualization of the gas–liquid flow in the annular slot and pictures of typical flow patterns to be obtained by a camera (4).

The column length from the inlet point of the two-phase flow to the column top was $L_0 = 0.6$ m, the annular gap thickness h between the cyclinders was 0.68 mm and the internal cylinder diameter was $D = 0.15$ m.

The water flow rate was measured and regulated using a turbine probe (5). The air flow rate was measured by the pressure drop at the orifice plates (6). Air at the temperature of the water directly entered the entrance chamber of the working section in which an air-distribution grid with holes was installed. The mixture temperature at the entrance was ~20°C. The experiments were performed at superficial velocities of $U_{G,S} = 0.035$ to 45 m/s (air) and $U_{L,S} = 0.4$ to 4.0 m/s (water).

The pressure drop was measured at the length $L = 0.53$ m. Static pressure measurements were performed in the entrance chamber and before the flow rate diaphragm. Pressure pulsations in the annular slot as well as in the entrance and exit chambers of the working section were measured using a high-frequency piezoelectric probe with a detector frequency up to 100 kHz (Nakoryakov *et al.* 1989). The gas and water temperatures were regulated by thermocouples. Data acquisition and processing were performed by a microcomputer.

STRUCTURE OF THE GAS–LIQUID FLOW IN THE NARROW ANNULAR CHANNEL

The gas and liquid phases in the flow form a large number of flow patterns. The flow patterns and the structure of the two-phase flow usually depend on the phase superficial velocities, the gas and liquid properties, the conditions at the entrance and the shape and size of the working section. Possible structures for the two-phase flow in the narrow annular channel are presented in figures 2 and 3.

When the ratio of the superficial velocities of the gas and liquid phases is < 10, the gas phase is distributed as bubbles in the liquid, their size usually being greater than the channel width. Bubbles of such large size in two-phase flow are referred to as Taylor bubbles. There is, however,

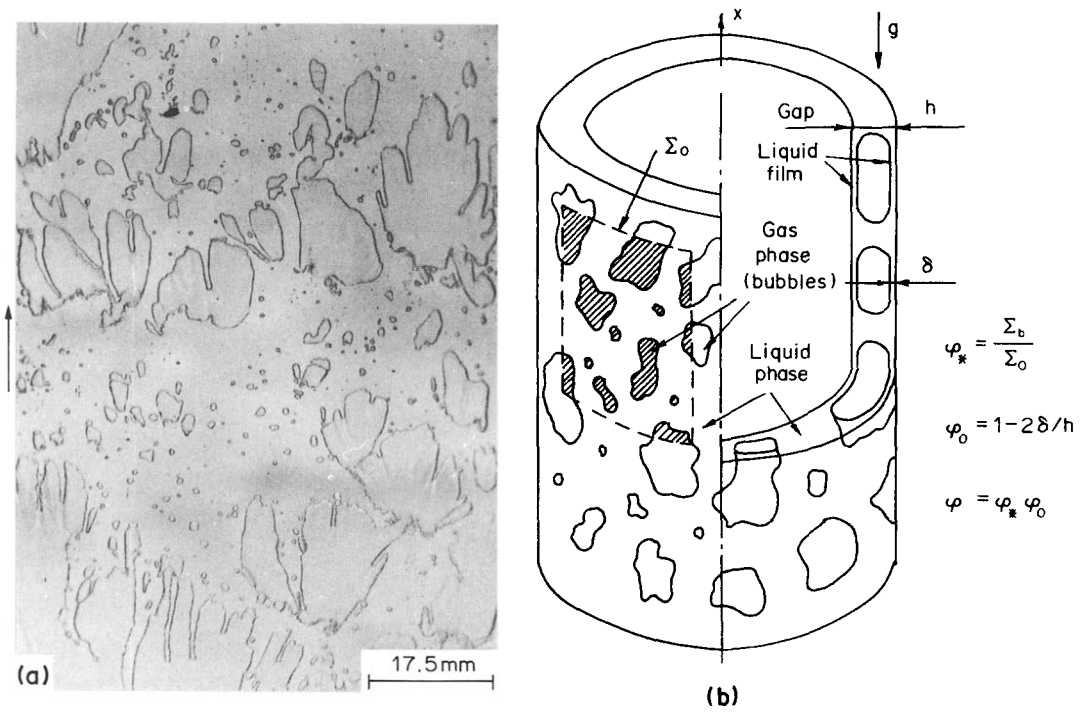

Figure 2. Structure of the bubble flow in the narrow annular channel at $U_{G,S}/U_{L,S} < 10$. (a) Photograph of the bubble flow ($U_{G,S} = 7.3$ m/s, $U_{L,S} = 2.07$ m/s). (b) Bubble flow geometry. Σ_0 is the lateral surface element and Σ_b is the part of the lateral surface element occupied by the gas phase.

a great difference between Taylor bubbles in the narrow annular channel and the tube: a bubble occupies a part of the annular channel only, whereas the liquid moves not only as a plug between the bubbles but forms a continuous phase through the entire channel length (Kelessidis & Dukler 1989).

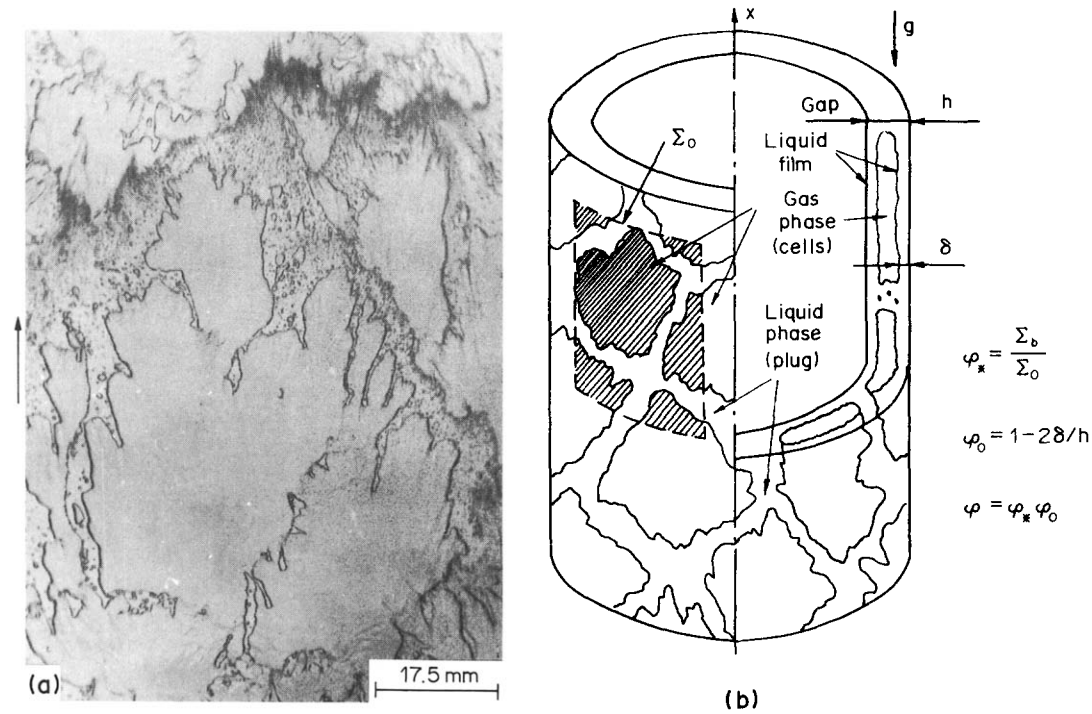

Figure 3. Structure of the cell flow in the narrow annular channel at $U_{G,S}/U_{L,S} > 10$. (a) Photograph of the cell flow ($U_{G,S} = 11.6$ m/s, $U_{L,S} = 0.85$ m/s). (b) Cell flow geometry. Key as in figure 2(b).

For an annular channel with a gap thickness less than the capillary constant, bubbles in the flow have very different sizes. The size distribution of Taylor bubbles in a narrow annular channel is related to the mechanism of their motion. For small distances between the channel walls and small liquid velocities the capillary forces at the gas–liquid interface are large and hinder the motion of Taylor bubbles [figure 2(b)]. This occurs at a small gas bubble, when the capillary number $N_C^* = (U_L \mu_L/\sigma)(l/h)$, which deals with the ratio of the hydrodynamical pressure drop over the bubble length l ($\Delta P_l = U_L \mu_L l/k$, where $k = h^2/12$ is the permeability, U_L is the liquid velocity and μ_L is the liquid dynamic viscosity) to the capillary pressure jump at the interface ($P_C = 2\sigma/h$), is <0.1 (Kopf-Sill & Homsy 1988). Then the bubble velocity can be much less than the liquid velocity U_L. For bubbles of greater size, when the pressure drop along the bubble length is commensurable with the capillary pressure jump and the capillary number reaches values close to 0.1, the bubble velocity abruptly increases with strong dependence upon N_C^* (Kopf-Sill & Homsy 1988), i.e. on the bubble size. If the bubble size is so great that $N_C^* \gg 0.1$, then the capillary forces are small and the balance between the pull from the surrounding fluid flow and the friction force due to the local flow in the fluid surrounding the bubble defines the bubble velocity. For an almost circular bubble the added mass is approximately equal to its volume multiplied by the liquid density and the bubble velocity up to a factor of 2 higher than the liquid velocity (Kopf-Sill & Homsy 1988). These features of bubble motion in narrow channels result in a large non-stationary of bubble size when $N_C^* > 0.1$. Bubbles with a relative velocity higher than the liquid velocity pick up smaller bubbles like a scraper [figure 2(a)] and grow rapidly. At the same time, at large relative velocities of the bubbles the interphase boundary becomes unstable with respect to perturbations of finite amplitude and bubbles start to split (Liang 1986) and break up [figure 2(a)]. Thus, the two-phase flow pattern observed in figure 2(a) showing Taylor bubbles of different size is a result of interaction of the bubbles and their coalescence and fragmentation.

If the ratio of the gas and liquid superficial velocities is >10, then the bubble size and density is so high that a non-stationary cell structure with liquid plugs appears [figure 3(a, b)]. These plugs separate the gas filling the cells with a thin liquid film at the gap walls and are transferred by gas flow, such as large disturbance waves in annular flow in pipes (Hall-Taylor *et al.* 1963; Sekoguchi *et al.* 1985). The liquid plugs are unstable, they are destroyed and reform with the same size. When plug destruction occurs, the liquid passes in to the film increasing its thickness. As a result, disturbance waves form on the film, they grow and after overlapping with the liquid at gaps opposite the wall form liquid plugs. These plugs cells with gas and move with a velocity close to that of the gas flow. Capillary forces prevent the plugs from being destroyed but, nevertheless, the cells are unstable and both the destruction of old plugs and the formation of new ones are observed. For a channel with large circumference the disturbance waves are usually curved (Azzopardi *et al.* 1983), some parts being farther downstream than others, and as a result of its interaction the cell structure of the two-phase flow is maintained.

FLOW PATTERN MAP

The map of the two-phase flow pattern in the narrow annular channel is presented in figure 4. Three typical flow structures can be seen: (1) flow with small bubbles whose size is less than the channel width; (2) flow with large Taylor bubbles close to the emulsion flow; and (3) flow with the cell structure of liquid plugs. The first type of flow is observed at superficial liquid velocities >2 m/s (points 1 in figure 4). At such velocities the flow is turbulent and small bubbles are created when large bubbles are broken up by turbulent forces (Kelessidis & Dukler 1989). A maximum stable diameter of the bubble can be obtained from the balance between surface tension and turbulent pulsations and is given by (Hinze 1955):

$$d_{max} = 0.725\left(\frac{\sigma}{\rho_L}\right)^{3/5}(\epsilon_d)^{-2/5}, \qquad [1]$$

where ϵ_d is the energy dissipation rate per unit mass. At low gas content the energy dissipation rate in the two-phase flow is close to that in the single-phase flow and is given by

$$\epsilon_d = \left(\frac{dP}{dx}\right)\frac{U_L}{\rho_L}. \qquad [2]$$

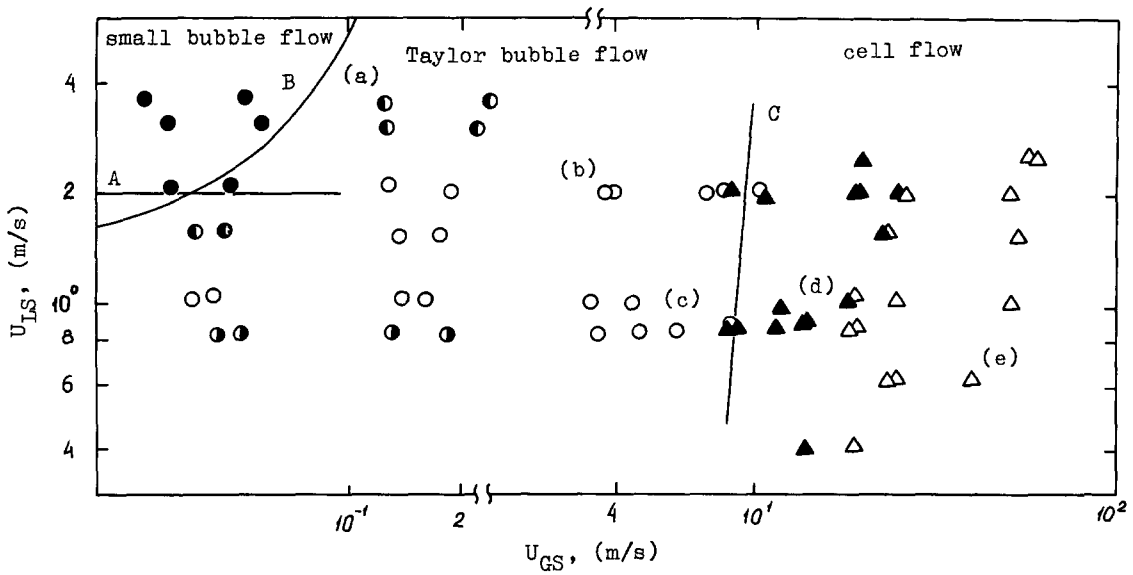

Figure 4. Flow pattern map: ●, small bubble flow (a); ◐, small bubble and Taylor bubble flow (b); ○, Taylor bubble flow (c); ◑, non-splitting Taylor bubble flow (d); ▲, △, cell flow (cells without ripples and cells with ripples, respectively) (e).

The friction factor for the single-phase flow in the annular channel equals $\lambda = 0.146/\mathrm{Re}_L^{0.25}$ (Sadatomi *et al.* 1982), where $\mathrm{Re}_L = U_L h \rho_L / \mu_L$ and the pressure gradient

$$\frac{dP}{dx} = \lambda \frac{\rho_L U_L^2}{2h}. \qquad [3]$$

The two-phase flow with small bubbles is stable if bubbles move along a straight line with similar velocities. The probability of bubble coalescence in such a flow is small and the volume gas content can exceed 0.25 without the transition to slug flow (Kelessidis & Dukler 1989). Bubbles smaller than the gap thickness move in a straight line if their diameter is less than the critical one given by Brodkey (1967):

$$d_{crit} = \left[\frac{0.46}{(\rho_L - \rho_G)g}\right]^{1/2}.$$

For narrow channels with a gap of $< 10^{-3}$ m, the critical size can be larger than the gap thickness and the capillary forces for bubbles with $h < d < d_{crit}$ result in a strong dependence of the bubble velocity on their size. This increases the probability of bubble coalescence and the flow with small bubbles is stable in this case if the bubble size after their destruction is less than the gap thickness. At $d_{max} = h$ the above considerations give the critical flow rate,

$$U_{L,crit} = \left\{\frac{0.725}{h}\left(\frac{\sigma}{\rho_L}\right)^{3/5}\left[\frac{0.073}{h}\left(\frac{\mu_L}{\rho_L h}\right)^{1/4}\right]^{-2/5}\right\}^{11/10}, \qquad [4]$$

provided that $U_{L,crit}$ corresponds to the turbulent flow developed in the channel ($\mathrm{Re}_L > 10^3$) (Sadatomi *et al.* 1982).

The critical liquid velocity for this system is 2 m/s (line A in figure 4). This value corresponds to the velocity at which turbulent flow appears in the channel, since [4] gives a smaller value of the critical velocity. For superficial gas velocities < 0.05 m/s and liquid velocities greater than the critical one, the bubble coalescence is small and flow with small bubbles is observed. High velocity gradients over the gap width can nevertheless lead to different velocities for the bubbles and their coalescence occurs at high gas velocities, resulting in the formation of Taylor bubbles. Line B in figure 4, determined experimentally, separates flow patterns with small and Taylor bubbles.

The flow with Taylor bubbles exists in the wide range of gas phase velocities—figures 4 and 5(b, c). When the velocity increases, the bubble size grows due to the coalescence of large bubbles.

At gas phase velocities 10 m/s the bubble size is so large that the liquid is localized in plugs between the bubbles and a cell flow pattern occurs—figure 5(d, e). Line C in figure 4 separates flow patterns with Taylor bubbles and cell structure. In the present system slug and annular flow patterns typical of two-phase flow in pipes have not been observed. The reason being the cell structure has smaller frictional losses than the annular one and energetically is more favourable. In order to show this, the pressure drops in the annular two-phase flow experimental data for the cell flow are compared. Pressure drops for the annular flow and data for the cell flow are presented in figure 6 for two superficial velocities. The pressure drops for the annular flow were calculated from the empirical relationship of Wallis (1969) for flow parameters in the mean cross-section A

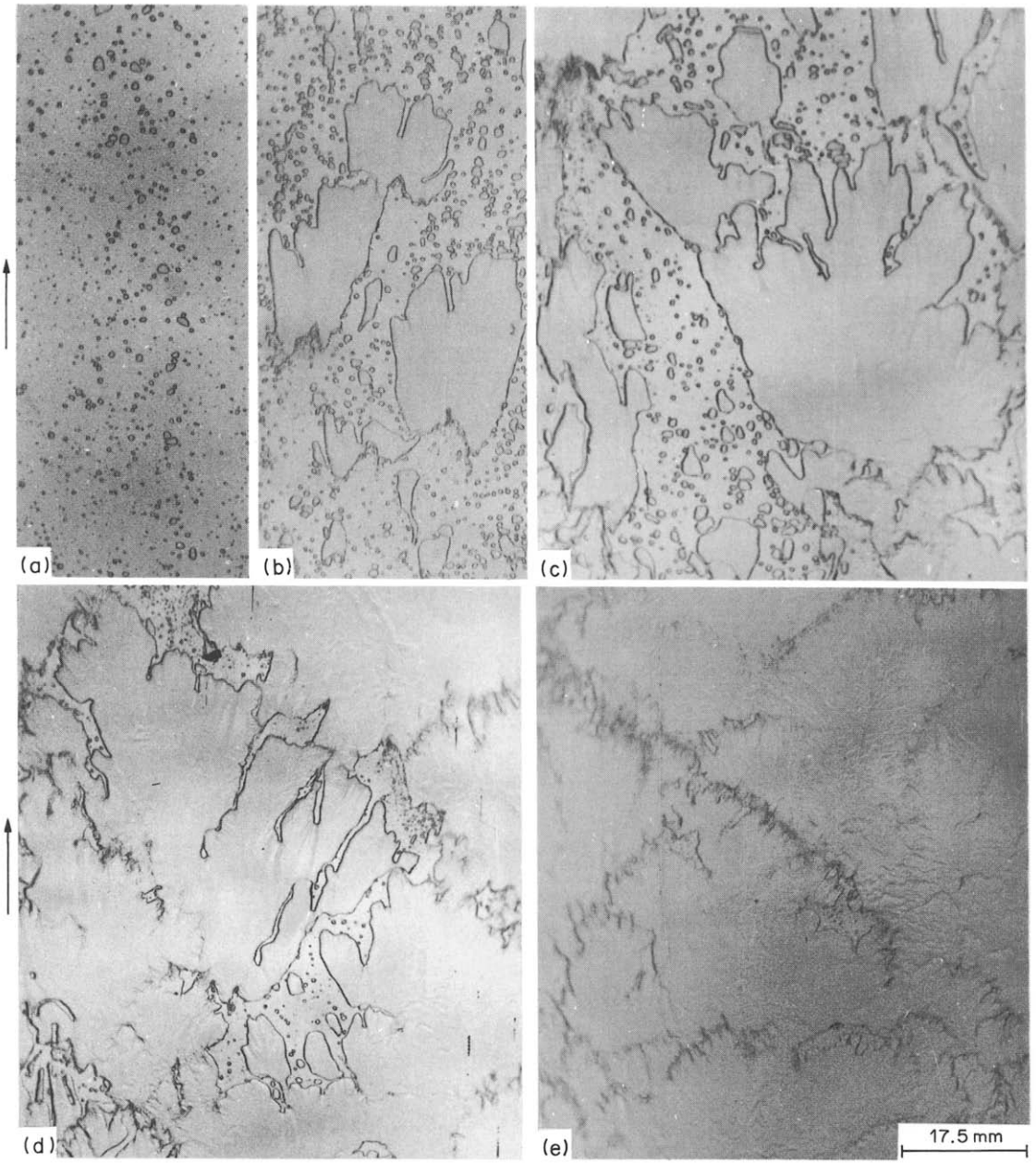

Figure 5. Photographs of the two-phase flow structure referring to (a)–(e) in figure 4. (a) Structure of small bubble and Taylor bubble flow ($U_{G,S} = 0.12$ m/s, $U_{L,S} = 3.07$ m/s). (b, c) Taylor bubble flow ($U_{G,S} = 3.874$ m/s, $U_{L,S} = 2.07$ m/s and $U_{G,S} = 6.06$ m/s, $U_{L,S} = 0.85$ m/s, respectively). (d, e) cells without ripples and with ripples respectively ($U_{G,S} = 13.3$ m/s, $U_{L,S} = 0.86$ m/s and $U_{G,S} = 38.6$ m/s, $U_{L,S} = 0.61$ m/s, respectively).

of the channel (figure 1), substituting the hydraulic equivalent diameter $D_h = 2 \cdot h$ for the tube diameter:

$$\Delta P = \frac{(\rho_{G,A} U_{G,A})^2 L}{2h\rho_{G,A}} \lambda_{G,A}\left(1 + 360\frac{\delta_A}{2h}\right) \quad [5]$$

where L is the channel length, δ_A is the film thickness, $U_{G,A} = U_{G,S}/(1 - 2\delta_A/h)$ is the gas velocity in the cross-section A and $\lambda_{G,A}$ is the gas friction factor. For laminar and turbulent flows in the narrow annular channel, the friction factors are

$$\lambda_{K,l} = \frac{24}{\mathrm{Re}_K} \quad [6]$$

and

$$\lambda_{K,t} = \frac{0.146}{\mathrm{Re}_K^{0.25}}, \quad K = \mathrm{G, L}, \quad [7]$$

where $\mathrm{Re}_K = U_K h \rho_K / \mu_K$, U, μ, G and L are the Reynolds number, velocity, dynamic viscosity, gas and liquid, respectively.

The thickness of a thin laminar film under the influence of friction caused by the cocurrent gas flow can be written, assuming that the film is not accelerated, as (Gilchrist & Naom 1987):

$$\delta = \frac{2\mu_L U_{L,f}}{\tau_i}, \quad [8]$$

where

$$\tau_i = 0.25 \lambda_G \rho_G U_G^2. \quad [9]$$

Here $U_{L,f} = U_{L,S} h/2\delta$ is the liquid velocity averaged over the film thickness and τ_i is the interfacial shear stress at the gas–liquid boundary in the narrow annular channel. From [8] and [9] one obtains the film thickness in the annular flow:

$$\frac{\delta_A}{h} = \sqrt{\frac{4U_{L,S}\mu_L\left(1 - \frac{2\delta_A}{h}\right)^2 \rho_{G,A}}{h\lambda_{G,A}\left(1 + \frac{360\,\delta_A}{h}\right)(\rho_{G,A} U_{G,S})^2}}. \quad [10]$$

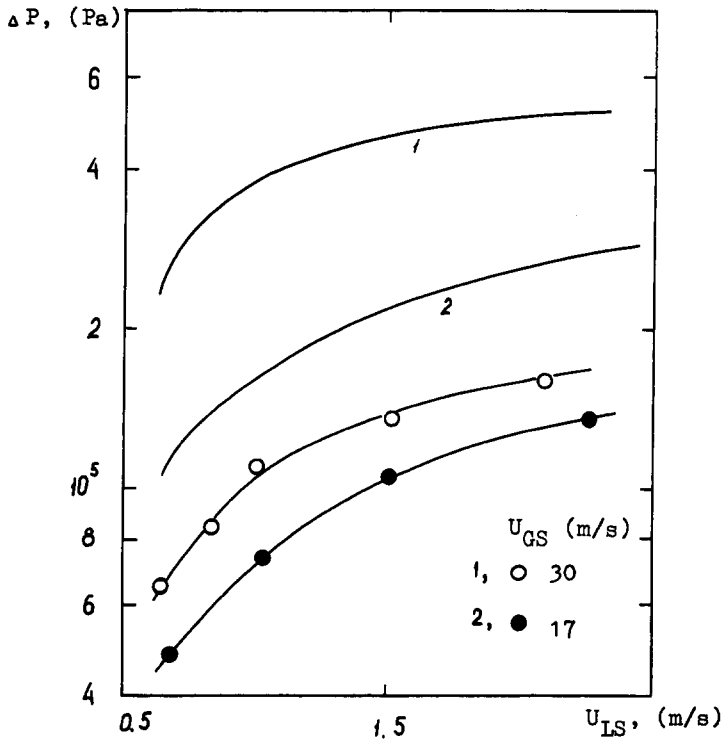

Figure 6. Pressure drop in an annular channel; 1,2—calculation according to [5].

From [5] and [10] one can obtain a pressure drop ΔP; iterations are necessary for its calculation since $\rho_{G,A}$ depends on the pressure in the cross-section A. The flow rate in our system is much less than the velocity of sound and the gas is isothermally expanded. Therefore, to calculate the gas density the relationship $\rho_{G,A} = \rho_0 P_A / P_0$ has been used, where ρ_0 is the gas density at atmospheric pressure P_0 at the channel exit and $P_A = P_0 + \Delta P/2$ is the pressure in the cross-section A (figure 1).

As follows from figure 6, frictional losses in annular flow can be smaller than in cell flow only at very small liquid velocities, $\ll 0.5$ m/s. It is here that one can expect the annular flow pattern.

The main cause of the large frictional losses in annular two-phase flow is the waves at the interface surface, especially the disturbance waves (Hall-Taylor *et al.* 1963; Hewitt & Hall-Taylor 1970). The large disturbance waves increase the dissipation of the turbulent energy in the gas core, and frictional losses increase considerably in comparison with those in flow with a smooth film. For cell flow the greater part of the annulus is occupied by the gas phase with a film at the gap walls [figure 3(b)], and the cells are divided by liquid plugs. The plugs concentrate in the liquid phase, making the film at the gap walls thinner and the liquid flow rate at the film small. The film in most cases is nearly wavy, with the exception of flows for superficial gas velocities of >20 m/s [figure 5(e)]. In such cases, the film within the cells is covered with ripples, as observed by Hall-Taylor *et al.* (1963) and by Azzopardi *et al.* (1983) in larger diameter tubes, but nevertheless large disturbance waves are absent. These waves result from the destruction of plugs and then transform into liquid plugs again.

Since the waves inside cells and Taylor bubbles are small the frictional losses inside them are close to those for a gas in a smooth channel. Therefore, the main frictional losses are related to the motion of liquid plugs and the local pressure in the channel is strongly pulsating. Pressure pulsations were measured at a distance of 0.035 m from the channel entrance (figure 1) and strongly correlate with the passage of liquid plugs. A similar correlation has also been observed for pressure pulsations measured in the channel at a distance of 0.035 m from the exit. Nevertheless, because the energy dissipation inside the cells is small, the total frictional losses in cell flow are less than those in annular flow (figure 6).

PRESSURE DROPS IN ANNULI

An attempt was made to correlate the present data by means of the Lockhart & Martinelli (1949) parameters, defined by

$$\Phi_L = \sqrt{\frac{\left(\frac{dP}{dx}\right)_f}{\left(\frac{dP}{dx}\right)_{fL}}} \qquad [11]$$

and

$$X = \sqrt{\frac{\left(\frac{dP}{dx}\right)_{fL}}{\left(\frac{dP}{dx}\right)_{fG}}}, \qquad [12]$$

where $(dP/dx)_f$ is the frictional loss for the two-phase flow, and $(dP/dx)_{fL}$ and $(dP/dx)_{fG}$ are those for the liquid and gas phase, respectively, flowing within the same channel. For a narrow annular channel, both $(dP/dx)_{fL}$ and $(dP/dx)_{fG}$ can be calculated for the laminar and turbulent flow from [6] and [7]. Figure 7 shows the experimental results. The data points are labelled according to the superficial liquid velocity and a combination of the modes of the superficial liquid and gas flow; the open symbols Φ_{Ll} correspond to the case where the flow of the gas phase alone is laminar, while filled symbols correspond to the case where the flow of the gas phase alone is turbulent. The flow of the liquid phase alone is always laminar. In addition, figure 7 presents the Lockhart & Martinelli (1949) Φ_{Ll} and Φ_{Llt} curves. The experimental data show large scatter and for the turbulent gas flow are considerably lower than the Lockhart–Martinelli curve. This is not typical of data processing

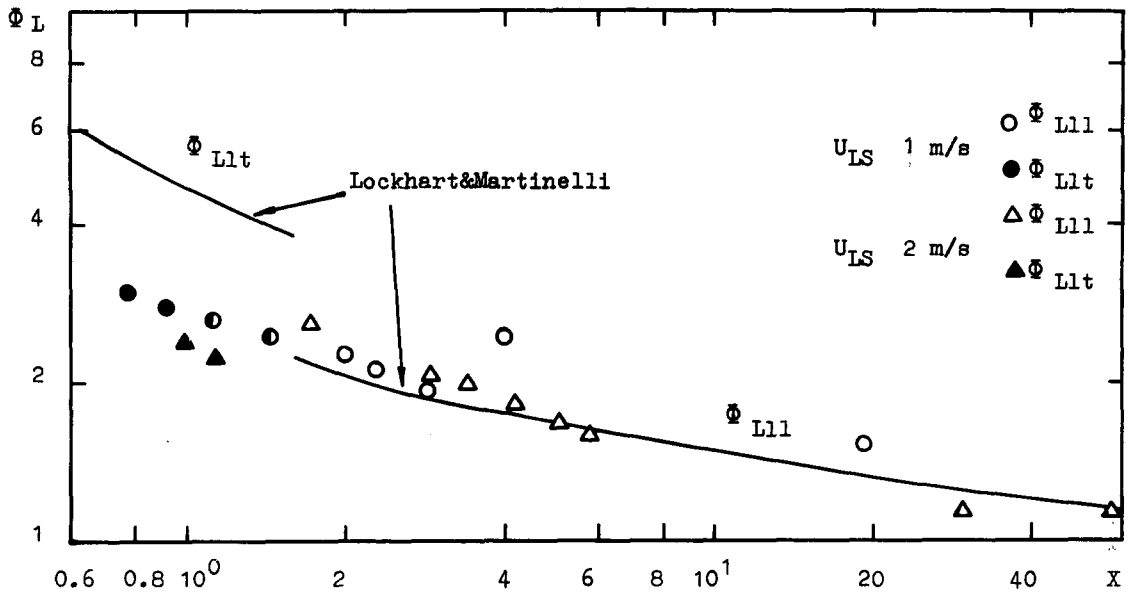

Figure 7. Two-phase frictional loss.

using Lockhart–Martinelli parameters, which usually describes well experimental data for different circular and noncircular channels (Sadatomi *et al.* 1982), and is probably due to new flow structures, in particular cell structure.

Visual observation of two-phase flow structures in a narrow annular channel shows that in our system the frictional losses are due to the friction in the liquid plugs and in the cells or Taylor bubbles. To determine this friction, consider the balance of forces for a stationary two-phase flow in an annular channel [figures 2(b) and 3(b)]. If there is no acceleration, an overall forces balance over the segment Δx gives (Kelessidis & Dukler 1989)

$$\frac{dP}{dx} + [\varphi\rho_G + (1-\varphi)\rho_L]g - \left(\frac{dP}{dx}\right)_f = 0, \qquad [13]$$

where φ is the volume gas content, $(dP/dx)_f$ is the frictional loss and the x-axis coincides with the flow direction. For narrow annular channels and high flow rates the frictional losses are large and the gravitational forces can be neglected.

Let φ_* be a specific lateral surface occupied by the gas phase (including a liquid film) [figures 2(b) and 3(b)]. The frictional losses in cells or Taylor bubbles for a thin wavy film with $\delta^2/h^2 \ll 1$ are due mainly to the interfacial shear stress at the gas–liquid boundary, [9]. Taking into account that part of the lateral surface is occupied by cells or bubbles (figures 2 and 3), the total frictional losses can be expressed as

$$-\left(\frac{dP}{dx}\right)_f = \frac{2}{h}\left[(1-\varphi_*)\frac{\rho_L U_L^2}{4}\lambda_L + \varphi_*\frac{\rho_G U_G^2}{4}\lambda_G\right], \qquad [14]$$

where U_L and U_G are the mean liquid and gas velocities, λ_L is the liquid friction factor in plugs and λ_G is the gas friction factor. The liquid friction factor in gas bubbles for turbulent and laminar flow can be calculated from [6] and [7] for a Reynolds number determined from the mean liquid velocity $Re_L = U_L h\rho_L/\mu_L$. If gas moves in Taylor bubbles or cells with a mean velocity U_G, this velocity is related to the superficial gas velocity $U_{G,S}$ by

$$U_G = \frac{U_{G,S}}{\varphi_*\left(1-\frac{2\delta}{h}\right)} \qquad [15]$$

and the volume gas content is confined to the liquid film thickness δ in a bubble:

$$\varphi = \varphi_*\varphi_0, \qquad [16]$$

where

$$\varphi_0 = \left(1 - \frac{2\delta}{k}\right).$$

Similarly, the mean liquid velocity U_L is related to the superficial liquid velocity $U_{L,S}$ as follows:

$$U_L = \frac{U_{L,S}}{(1-\varphi_*)} - \frac{2U_{L,f}\delta}{h}. \quad [17]$$

Combining [8] and [16], one obtains

$$U_L = \frac{U_{L,S}}{(1-\varphi_*)} - \frac{1}{4}\left(\frac{\delta}{h}\right)^2 \frac{\lambda_{G,i}\rho_G U_G^2 h}{\mu_L}. \quad [18]$$

For thin films with $(\delta/h)^2 \ll 1$ the second term on the r.h.s. of [18] is usually much smaller than the first one and can be neglected.

The surface between the liquid and gas in liquid plugs is a meniscus which exists in the space between the channel walls. When the surface moves, this meniscus forms a film after it. This problem is similar to that of Landau & Levich (1942) of a film remaining on the vertical plate. At small meniscus velocities the film thickness follows the law of 2/3 for the capillary number $N_{CL} = U_L\mu_L/\sigma$, determined from the liquid velocity near the meniscus (Bretherton 1961). This law is no longer valid at $N_{CL} > 10^{-2}$, however Reinalt & Saffman (1985) published numerical calculations of film thickness up to $N_{CL} = 2$, consistent with their experimental data.

In the data analysis it is useful to introduce the mean flow rate mixture density

$$\hat{\rho} = \rho_L(1-\beta) + \rho_G\beta, \quad [19]$$

where

$$\beta = \frac{U_{G,S}}{U_m}. \quad [20]$$

Here β is the flow rate gas content and U_m is the mixture velocity,

$$U_m = U_{G,S} + U_{L,S}. \quad [21]$$

Defining the flow friction factor as

$$\lambda_m = \frac{\left(\frac{dP}{dx}\right)2h}{\hat{\rho}U_m^2} \quad [22]$$

and combining [22] and [14], we obtain

$$\lambda_m = \lambda_L \frac{\rho_L U_L^2}{\hat{\rho}U_m^2}(1-\varphi_*) + \lambda_G \frac{\rho_G U_G^2}{\hat{\rho}U_m^2}\varphi_*. \quad [23]$$

(a) Turbulent flow of liquid and gas

Combining [23] with [15], [18] and [7] gives

$$\lambda_m = \frac{0.146}{Re_m^{0.25}} \cdot \frac{\rho_L(1-\beta)^{1.75}}{\hat{\rho}(1-\varphi_*)} + \frac{0.146}{Re_{G,S}^{0.25}} \cdot \frac{\rho_G\beta^2}{\hat{\rho}\varphi_0^{1.75}\phi_*^{0.75}}, \quad [24]$$

where the Reynolds number $Re_m = U_m h\rho_L/\mu_L$ is determined from the mixture velocity and liquid viscosity.

(b) Turbulent liquid flow and laminar gas flow

Combining [23] with [15], [18], [16] and [7] gives, in this case,

$$\lambda_m = \frac{0.146}{Re_m^{0.25}} \cdot \frac{\rho_L(1-\beta)^{1.75}}{\hat{\rho}(1-\varphi_*)^{0.75}} + \frac{24}{Re_{G,S}} \cdot \frac{\rho_G\beta^2}{\hat{\rho}\varphi_0}. \quad [25]$$

At atmospheric pressure and a flow rate gas content of $\beta < 0.95$, one can neglect the second term on the r.h.s. of [24] and [19]. Then for two-phase flow in which the velocities of the gas bubbles

are equal to the mean velocity and the thickness of the liquid film is small, $\varphi_0 \approx 1$, the flow rate gas content β is equal to that of the volume φ (homogeneous flow), so that [24] gives

$$\lambda_m = \frac{0.146}{\mathrm{Re}_m^{0.25}}. \qquad [26]$$

Such a flow can occur for weakly interacting Taylor bubbles when their splitting and break up prevents the bubbles from having a velocity larger than that of the liquid [figure 5(b)].

(c) Laminar flow of liquid and gas

Combining [23] with [15], [18] and [6] gives

$$\lambda_m = \frac{24}{\mathrm{Re}_m} \cdot \frac{\rho_L(1-\beta)}{\hat{\rho}} + \frac{24}{\mathrm{Re}_{G,S}} \cdot \frac{\rho_G \beta^2}{\hat{\rho}\varphi_0}. \qquad [27]$$

At atmospheric pressure and $\beta < 0.95$ one can neglect the second term on the r.h.s. of [27] and [19], as in the case of turbulent flow. In this case the friction factor is independent of the phase slip and can be described by the same dependence as the liquid flow with the mixture velocity.

(d) Experimental results

Data on pressure drops have been obtained for a wide range of possible flow structures in the narrow annular channel for superficial gas velocities at the channel exit ranging from 0.035 to 45 m/s and liquid velocities from 0.4 to 4.0 m/s. The results are presented in figure 8 in λ_m, Re_m coordinates for different superficial liquid velocities. The mixture velocity and its mean flow rate density were determined for the pressure in the mean cross-section A of the channel (figure 1) $P_A = P_0 + \Delta P/2$, assuming that gas expands isothermally and $\rho_{G,A} = \rho_0 P_A/P_0$ and $U^A_{G,S} = U^0_{G,S} P_0/P_A$; here ρ_0 and $U^0_{G,S}$ are the pressure and superficial velocity at atmospheric pressure. In addition, correlations are presented for laminar, [6], and turbulent, [7], liquid flows ($U_m = U_L, \beta = 0$). Experimental points for single-phase flow are well-approximated by the well-known dependence for laminar flow and come to the dependence for turbulent flow. For two-phase flow in the range of Re_m from 700 to $3 \cdot 10^3$, the bubbles produce turbulent pulsations and one observes a developed turbulent flow instead of a transient mode. In this range of Re_m small bubbles of a size less than the

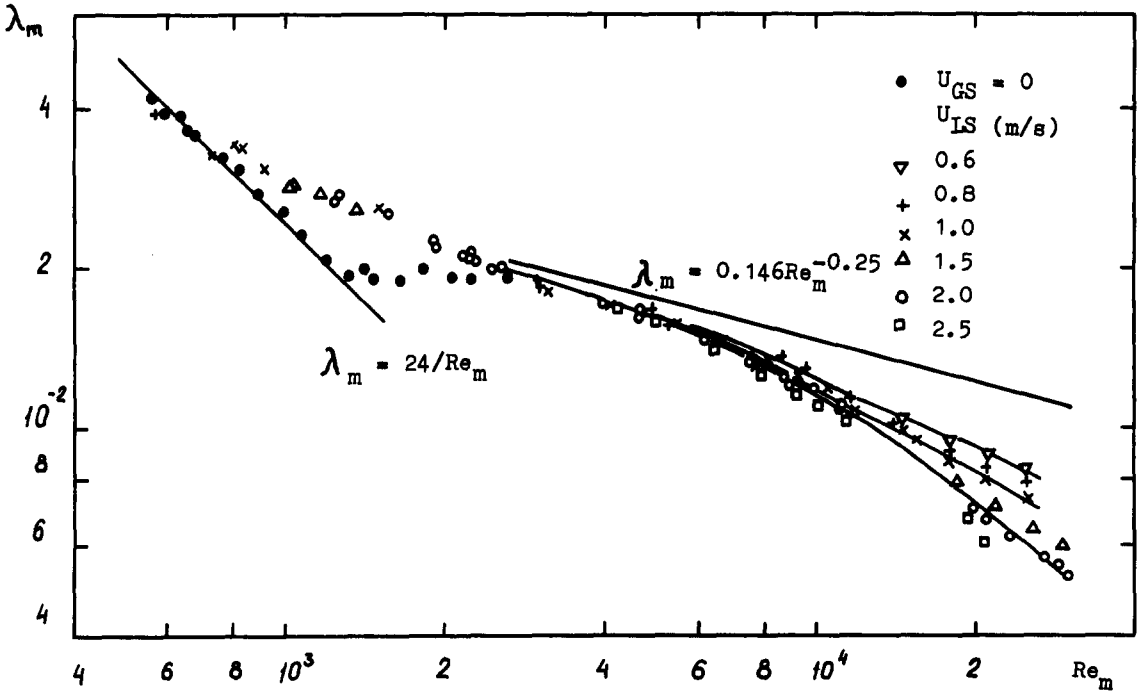

Figure 8. Friction factor and Reynolds number relationship; 1,2,3—calculation according to [24] and [25] at $U_{L,S} = 0.6$, 1.0 and 2.0 m/s, respectively.

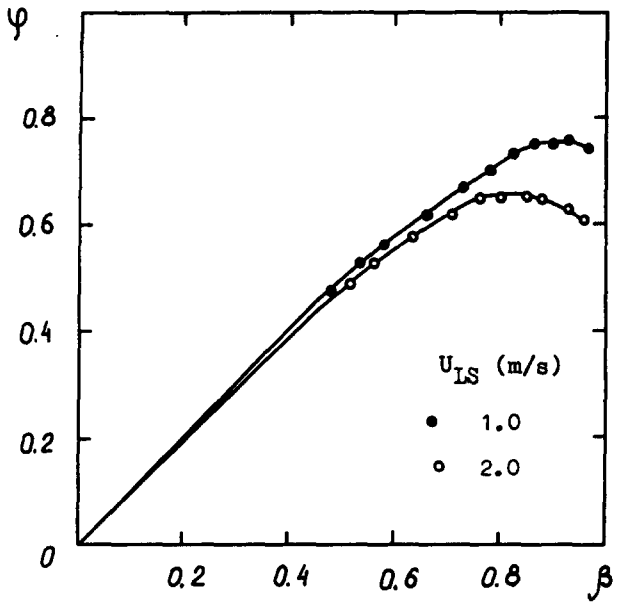

Figure 9. Volume gas content vs gas flow rate.

channel width are observed in the flow as well as weakly interacting Taylor bubbles [figure 5(a, b)]. Such bubbles have a velocity close to that of the liquid and experimental points are well-described by [26], and at $Re_m = 700$ are close to [27] for laminar gas and liquid flow.

When $Re_m > 4 \cdot 10^3$, the process of bubble coalescence dominates over their break-up [figure 5(c, d)] and the gas velocity becomes larger than that of the liquid. In this case, one cannot use correlation [26] and the experimental points divide into groups depending on the superficial liquid velocity, the effect being stronger at large Re_m.

Correlations [24] and [25] do not allow calculation of the friction factor λ_m to be performed since the values of φ_* and φ_0 are unknown. Let us assume that [24] and [25] can be used and determine φ_* and φ_0, as well as the mean velocities of both phases, from the experimental data. Calculation of φ_* and φ_0 requires iterations. First, for an arbitrary φ_0 and λ_m^e determined experimentally one calculates φ_* from [24] or [25]. Then equations [15] and [18] give the mean velocities of the liquid

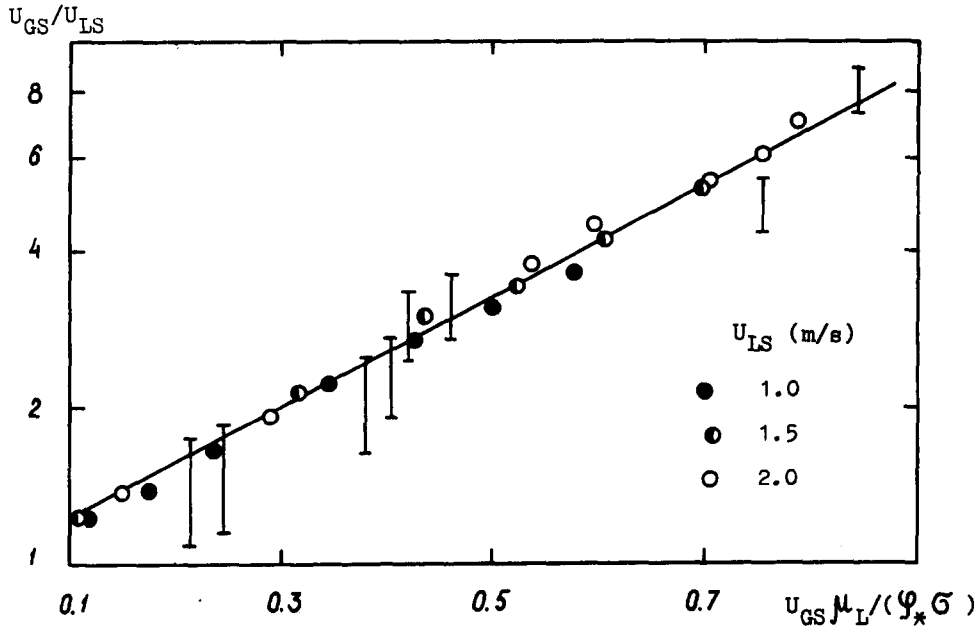

Figure 10. Ratio of the gas to liquid superficial velocities vs the modified capillary number.

U_L and gas U_G and from the calculations of Reinalt & Saffman (1985) one can obtain the thickness of the liquid film δ and φ_0. If the value of φ_0 thus determined does not coincide with its initial value, the calculation is repeated until the deviation is $<10\%$. The results are shown in figures 9 and 10. Figure 9 presents the volume gas content $\varphi = \varphi_* \varphi_0$ for different values of β obtained at two superficial liquid velocities. The volume content has a maximum corresponding to the transition from two-phase flow with Taylor bubbles to cell flow. The superficial phase velocities at which the volume content φ has a maximum can be used to identify the transition to cell flow and are shown by the line C in figure 4. The decrease in the gas content φ when β increases in cell flow is due to the destruction of plugs and the growth in the relative gas–liquid velocity.

The results of the calculations of the ratio of the mean gas and liquid velocities are shown in figure 10. For the complete range studied the gas and liquid velocities are described by the empirical correlation

$$\frac{U_G}{U_L} = \exp(2.4\, N_{C*}), \qquad [28]$$

where $N_{C*} = U_{G,S}\mu_L/\varphi_* \sigma$ is the modified capillary number. This number determines the stability against the destruction of liquid plugs trapping the gas in the cells and preventing it from moving faster than the liquid. At large superficial gas velocities the capillary forces cannot keep the gas completely in the cells and the ratio of the mean velocities of gas and liquid becomes larger.

In addition, figure 10 shows experimental data on this ratio in two-phase flow of the cell structure obtained by another method. This used the fact that the motion of liquid plugs and the gas flow following them causes pressure pulsations at the channel wall.

The period of pressure pulsations is equal to the time it takes for one cell to be completely replaced by another at the probe location. Then the average liquid velocity in plugs forming cell boundaries is a ratio of the average cell length to the average period of pressure pulsations. The average cell length was determined from the flow pictures. The large scatter of cell lengths and pulsation periods in one experiment results in large uncertainties in the mean liquid velocity. Taking this into account, we used the superficial gas velocity instead of the mean gas velocity for the data of figure 10.

Combining [28], [15] and [18] gives

$$\frac{U_{G,S}}{U_{L,S}} \frac{(1-\varphi_*)}{\varphi_* \varphi_0} = \exp\left(2.4 \frac{U_{G,S}\mu_L}{\varphi_* \sigma}\right). \qquad [29]$$

Equations [29], [18] and [15], and the correlations [24] and [25] as well as the numerical results of Reinalt & Saffman (1985) for the liquid film thickness allow the calculation of the friction factor using iterations in φ_0 as shown earlier. In addition to experimental data, figure 8 presents the results of the calculations of correlations [24] and [25] at two superficial liquid velocities $U_{L,S} = 1$ and 2 m/s. For the entire range of Re_m, the experimental points are well described by the calculated results.

CONCLUSIONS

Data have been presented which allow the identification of different flow patterns in a narrow annular channel with a gap thickness less than the capillary constant. For large phase velocities, two-phase flow with Taylor bubbles and a cell flow with liquid plugs is typical. Slug and annular flow patterns have not been observed. A mathematical model has been developed, based on the physical mechanisms suggested for different flow patterns, which can predict the friction factor in a narrow annular channel. A method to calculate the friction factor based on the obtained empirical correlation of the mean gas-to-liquid velocity ratio has been suggested. The calculations agree with the experimental data.

REFERENCES

AZZOPARDI, B. J., TAYLOR, S. & GIBBONS, D. B. 1983 Annular two-phase flow in a large diameter tube. Presented at the *Int. Conf. on Physical Modelling of Multi-phase Flow*, Coventry, England, Paper F4.

BRETHERTON, F. P. 1961 The motion of long bubbles in tubes. *J. Fluid Mech.* **10,** 166–188.

BRODKEY, R. C. 1967 *The Phenomena of Fluid Motions.* Addison-Wesley, Reading, MA.

CAETANO, E. F., SHOHAM, O. & BRILL, J. P. 1989a Upward vertical two-phase flow through an annulus. Part I: single-phase friction factor, Taylor bubble rise velocity and flow pattern prediction. In *Multiphase Flow—Proc. 4th Int. Conf.*, pp. 301–330. BHRA, Cranfield, England.

CAETANO, E. F., SHOHAM, O. & BRILL, J. P. 1989b Upward vertical two-phase flow through an annulus. Part II: modelling bubble, slug and annular flow. In *Multiphase Flow—Proc. 4th Int. Conf.*, pp. 331–362. BHRA, Cranfield, England.

GILCHRIST, A. & NAOM, K. 1987 Co-current flow of air thin liquid film in a vertical tube. In *Multiphase flow—Proc. 3rd Int. Conf., The Hague, The Netherlands*, pp. 97–103, BHRA, Cranfield, England.

HALL-TAYLOR, N. S., HEWITT, G. F. & LACEY, P. C. M. 1963 The motion and frequency of large disturbance waves in annular two-phase flow of air–water mixtures. *Chem. Engng Sci.* **18,** 537–552.

HEWITT, G. F. 1982 Flow regimes. In *Handbook of Multiphase Systems* (Edited by HETSRONI, G.). Hemisphere, Washington, DC.

HEWITT, G. F. & HALL-TAYLOR, N. S. 1970 *Annular Two Phase Flow.* Pergamon Press, Oxford.

HINZE, J. O. 1955 Fundamentals of the hydrodynamic mechanism of splitting in dispersion processes. *AIChE Jl* **1,** 269–295.

KELESSIDIS, V. C. & DUKLER, A. E. 1989 Modeling flow pattern transitions for upward gas–liquid flow in vertical concentric and eccentric annuli. *Int. J. Multiphase Flow* **15,** 173–191.

KOPF-SILL, A. R. & HOMSY, G. M. 1988 Bubble motion in a Hele–Shaw cell. *Phys. Fluids* **31,** 18–26.

LANDAU, L. & LEVICH, B. 1942 Dragging of a liquid by a moving plate. *Acta Physiocochim. URSS* **7,** 42–47.

LIANG, S. 1986 Random walk simulations of flow in Hele–Shaw cells. *Phys. Rev.* **A33,** 2663–2674.

LOCKHART, R. W. & MARTINELLI, R. C. 1949 Proposed correlation of data for isothermal two-phase, two-component flow in pipes. *Chem. Engng Prog.* **45,** 39–48.

NAKORYAKOV, V. E., KUZNETSOV, V. V. & DONTSOV, V. E. 1989 Pressure waves in saturated porous medium. *Int. J. Multiphase Flow* **15,** 857–875.

REINALT, D. A. & SAFFMAN, P. G. 1985 The penetration of a finger into a viscous fluid in a channel and tube. *J. Scient. Statist. Comput.* **6,** 542–549.

SADATOMI, M., SATO, Y. & SARUWATARI, S. 1982 Two-phase flow in vertical noncircular channels. *Int. J. Multiphase Flow* **8,** 641–655.

SEKOGUCHI, K., TAKEISHI, M. & ISHIMATSU, T. 1985 Interfacial structure in vertical upward annular flow. *PhysicoChem. Hydrodynam.* **6,** 239–255.

WALLIS, G. B. 1969 *One-dimensional Two-phase Flow.* McGraw-Hill, New York.